




# Atomistic analysis of Auger recombination in *c*-plane (In,Ga)N/GaN quantum wells: Temperature-dependent competition between radiative and nonradiative recombination

Joshua M. McMahon <sup>1,2,\*</sup>, Emmanouil Kioupakis,<sup>3</sup> and Stefan Schulz <sup>1,2</sup>

<sup>1</sup>Tyndall National Institute, University College Cork, Cork T12 R5CP, Ireland

<sup>2</sup>Department of Physics, University College Cork, Cork T12 YN60, Ireland

<sup>3</sup>Materials Science and Engineering Department, University of Michigan, 2300 Hayward Street, Ann Arbor, Michigan 48109, USA

 (Received 21 October 2021; revised 20 March 2022; accepted 25 April 2022; published 12 May 2022)

We present an atomistic theoretical study of the temperature dependence of the competition between Auger and radiative recombination in *c*-plane (In,Ga)N/GaN quantum wells with indium (In) contents of 10%, 15%, and 25%. The model accounts for random alloy fluctuations and the connected fluctuations in strain and built-in field. Our investigations reveal that the total Auger recombination rate exhibits a weak temperature dependence; at a temperature of 300 K and a carrier density of  $n_{3D} = 3.8 \times 10^{18} \text{ cm}^{-3}$ , we find total Auger coefficients in the range of  $\approx 6 \times 10^{-30} \text{ cm}^6/\text{s}$  (10% In) to  $\approx 3 \times 10^{-31} \text{ cm}^6/\text{s}$  (25% In), thus large enough to significantly impact the efficiency in (In,Ga)N systems. Our calculations show that the hole-hole-electron Auger rate dominates the total rate for the three In contents studied; however, the relative difference between the hole-hole-electron and electron-electron-hole contributions decreases as the In content is increased to 25%. Our studies provide further insight into the origin of the “thermal droop” (i.e., the decrease in internal quantum efficiency with increasing temperature at a fixed carrier density) in (In,Ga)N-based light-emitting diodes. We find that the ratio of radiative to nonradiative (Auger) recombination increases in the temperature range relevant to the thermal droop ( $\geq 300 \text{ K}$ ), suggesting that the competition between these processes is not driving this droop effect in *c*-plane (In,Ga)N/GaN quantum wells. This finding is in line with recent experimental studies.

DOI: [10.1103/PhysRevB.105.195307](https://doi.org/10.1103/PhysRevB.105.195307)

## I. INTRODUCTION

Understanding radiative and nonradiative recombination processes in semiconductor materials and heterostructures (e.g., nanocrystals, quantum dots, and quantum wells) has attracted the attention of research for several decades [1–11]. One motivation for this is the insight it provides into the fundamental physical properties of semiconductors, and how these properties change between materials [6,7] and/or types of heterostructures [8,12,13]. Equally, this understanding is crucially important for designing (energy-)efficient light-emitting devices [3,12,14].

In recent years, high-efficiency nitride-based light-emitting diodes (LEDs), operating in the violet-blue spectral range, that utilize indium gallium nitride ((In,Ga)N) alloys have emerged [3,12,14,15]. Significant research efforts have been directed towards understanding the radiative and nonradiative recombination processes in these systems [9–12,14,16], since these are of particular relevance to the ‘efficiency droop’ (also known as “current droop”) i.e., the decrease in LED internal quantum efficiency (IQE) induced by high current density and “thermal droop” (i.e., the decrease in IQE with increasing device temperature even at a fixed current and/or carrier density) [17]. In general, experimental studies have revealed that nonradiative Auger recombination can be a significant contributor to the efficiency droop observed in nitride-based

LEDs [3,18–20], even though this effect is unusual for wide-band-gap materials [21]. While some studies have highlighted the presence [3] of Auger recombination, others have also quantified [22–24] this contribution. It is also important to note that although the thermal droop may have its origin in intrinsic processes, such as radiative and nonradiative recombination, it may also be caused by factors pertaining to charge carrier transport, e.g., carrier injection deficiencies, in nitride-based devices [25]. Therefore, calculating the temperature dependence of (nonradiative) Auger and radiative recombination rates in (In,Ga)N-based quantum wells (QWs) will shed light on the relevance of these processes to the thermal droop in (In,Ga)N-based light emitters and also provide insight into the fundamental properties of these wide-band-gap structures.

First-principles calculations targeting bulk (In,Ga)N systems have shown that alloy fluctuations play a major role in enabling strong Auger recombination, along with phonon-assisted processes [26]. Moreover, it has also been observed, both in theory and experiment, that (random) alloy fluctuations and the strong intrinsic built-in fields in *c*-plane (In,Ga)N/GaN QWs significantly affect the radiative recombination rate [27–29]. These factors make the properties of (In,Ga)N-based systems very different from other, more “conventional” group III-V based heterostructures. For instance, in QW structures utilizing the more “conventional” group III-V material GaAs, the radiative recombination rate, often described by the so-called *B* coefficient, decreases with increasing temperature, *T* [30,31]. In contrast, experimental

\*joshua.mcmahon@tyndall.ie

investigations reveal that in (In,Ga)N/GaN QW systems,  $B$  increases with increasing temperature [24].

To gain insight into the underlying origin of this behavior, from a theoretical viewpoint, large-scale, fully three-dimensional calculations are required to capture (i) realistic well widths, (ii) the GaN barrier material, (iii) (spontaneous and piezoelectric) polarization fields, and, of particular importance, (iv) (random) alloy fluctuations, which ideally should be accounted for on an atomistic level. Taking all of this into consideration, the corresponding simulation cells become very large ( $> 10\,000$  atoms), and are thus beyond the reach of “standard” density-functional theory (DFT) frameworks. As a consequence, the analysis of nonradiative Auger recombination in (In,Ga)N/GaN QWs must be carried out by means of semiempirical models. However, modified continuum-based calculations indicate a decrease in  $B$  with increasing temperature [25,32], in contrast to experimental data [24]. Recent calculations utilizing atomistic tight-binding (TB) models show that this increase in  $B$  is tightly linked to carrier localization effects in (In,Ga)N-based QWs [28,33] and that modified continuum-based models may underestimate the impact of alloy fluctuations on carrier localization effects [34].

However, there has not been an *atomistic* theoretical study that focuses on the temperature dependence of the Auger recombination rate in (In,Ga)N/GaN QWs so far. Previous theoretical studies mainly assume “ideal” (i.e., without alloy fluctuations) QW band structures [16,35], or employ modified continuum-based models [32,36,37], which (i) neglect the underlying atomistic structure, (ii) may underestimate carrier localization effects, and (iii) usually neglect information on higher-lying, empty electron and/or hole states [16]. For instance, the theoretical data in Refs. [32,35] indicate that the Auger recombination rate, described by the Auger coefficient,  $C$ , decreases with increasing temperature in  $c$ -plane (In,Ga)N/GaN QWs. This is consistent with the experimental data in Refs. [23,38] but stands in contrast to the theoretical results in Ref. [16] and the experimental data of Refs. [22,24,37] in which  $C$  increases with increasing temperature.

All of this highlights that there is still a large degree of uncertainty surrounding nonradiative Auger recombination processes and their temperature dependence in (In,Ga)N-based QWs. In this work we apply an atomistic TB model that we have previously used to describe the temperature dependence of the  $B$  coefficient, to gain insight into the temperature dependence of the Auger coefficients in  $c$ -plane (In,Ga)N/GaN QWs. In general our calculations show that the dominant contribution to the total Auger coefficient, independent of the In content in the well, is given by the hole-hole-electron ( $h$ - $h$ - $e$ ) process. However, the relative contribution from the electron-electron-hole ( $e$ - $e$ - $h$ ) process increases as the In content increases to 25%, although the total rate decreases on the whole as the In content increases. A decrease of the Auger coefficient with decreasing band gap (increasing In content) has also been seen in experiment [24,37]. We note that, in general, but especially at low temperatures ( $< 120$  K), the alloy microstructure can strongly affect the magnitude of the Auger coefficient. Overall, at a temperature of 300 K and a carrier density of  $n_{3D} = 3.8 \times 10^{18} \text{ cm}^{-3}$  we find total Auger coefficients in the range of  $\approx 6 \times 10^{-30} \text{ cm}^6/\text{s}$  (10% In) to  $\approx 3 \times 10^{-31} \text{ cm}^6/\text{s}$

(25% In). These coefficients are within the wide range of literature values and large enough to significantly impact the efficiency of (In,Ga)N-based light emitters [17]. In general, our calculations show that in the temperature range relevant to the *thermal* droop, the total Auger coefficients for different In contents exhibit a (slight) decrease with increasing temperature. Taking these findings into account, and considering our previously calculated temperature-dependent radiative recombination coefficients,  $B$  [28], at high temperatures ( $\gtrsim 300$  K), we find that the ratio of radiative to Auger recombination increases. These findings indicate that the Auger process is not a driving factor behind the thermal droop phenomenon observed in (In,Ga)N-based LED structures. Therefore, we conclude that other factors, e.g., carrier injection or defect-related processes, are more likely to be its origin. This conclusion is in line with recent experimental studies [25].

The paper is organized as follows. In the following section, Sec. II, we discuss the theory underlying the calculations. In Sec. III, we present the results before summarizing the work in Sec. IV.

## II. THEORY

In this section we give an overview of our theoretical framework. The TB model applied in our study and the underlying assumptions for the investigated QW structures are discussed in Sec. II A. The details of the Auger recombination rate calculations are given in Sec. II B.

### A. Electronic structure and quantum well model systems

In order to capture the strong carrier localization effects in (In,Ga)N alloys and (In,Ga)N/GaN QW systems [39,40], we use a three-dimensional, atomistic, nearest-neighbor,  $sp^3$  TB model. The full details of the theoretical framework are given in Refs. [41,42] and we only briefly summarize the main ingredients here. The TB model employed has previously been parametrized and benchmarked against hybrid-functional DFT (HSE-DFT). It should be noted that not only does the TB model used here show very good agreement with GaN and InN HSE-DFT bulk band structures for the lowest conduction and highest valence bands near the  $\Gamma$  point, but also for energetically higher- and lower-lying states and bands away from  $\Gamma$ , as presented in Ref. [41]; this is particularly significant for Auger calculations as the energetically higher- and lower-lying states are as important as the states near the band edges [26]. The model has then been further benchmarked for (In,Ga)N bulk and QW systems, over a wide In content range, against both DFT and experimental data [29,41]. To model (local) strain effects, arising from the lattice mismatch between InN and GaN in the (In,Ga)N QW region, a valence force field model [42] is used to obtain the relaxed atomic positions of the (In,Ga)N/GaN QW system. Polarization field fluctuations in the  $c$ -plane (In,Ga)N QWs considered here are evaluated on the basis of a local polarization theory [41].

In the following, we have targeted structures similar to those analyzed experimentally in Refs. [29,43]. As discussed in more detail in Ref. [29], all calculations have been carried out on simulation cells with a size of  $10 \times 9 \times 10 \text{ nm}^3$

[containing (In,Ga)N wells with widths on the order of 3 nm and the surrounding GaN barriers], with periodic boundary conditions; the system corresponds to  $32 \times 32 \times 20$  wurtzite unit cells. The results for electronic and optical properties obtained from our TB model are in good agreement with low-temperature experimental data, such as the photoluminescence (PL) peak positions and full width at half maximum (FWHM) values, on  $c$ -plane (In,Ga)N/GaN QWs with In contents ranging from 5% up to 25% [29]. For all of these studies the assumption of a random alloy has been made, in agreement with general atom probe tomography results on  $c$ -plane (In,Ga)N/GaN wells [44]. In our model we also allow for the “bleeding” of In atoms into the GaN barrier. However, we restrict this penetration of In atoms into the barrier material to a disklike region with a height of two monolayers (MLs), and a width of approximately 5 nm, following the experimental and theoretical work of Refs. [42,45,46]. Given that we assume a random alloy distribution of the In atoms in the QW region, the actual “shape” of the structural inhomogeneities (well width fluctuations) varies between different microscopic alloy configurations.

### B. Calculation of Auger recombination rate

In order to calculate the rate of Auger recombination in (In,Ga)N/GaN QWs, we broadly follow the method laid out in Ref. [26]. Using Fermi’s golden rule, the Auger recombination rate is given by

$$R = 2 \frac{2\pi}{\hbar} \sum_{1234} P(T) |M_{1234}|^2 \delta(\epsilon_1 + \epsilon_2 - \epsilon_3 - \epsilon_4). \quad (1)$$

In the case of other systems that lack symmetry breaking due to alloy fluctuations, the bold indices denote both band index and  $\mathbf{k}$  point. For the structures studied here, the bold indices run over the QW electron and hole states. The (temperature-dependent) prefactor  $P(T) = f_1(T)f_2(T)[1 - f_3(T)][1 - f_4(T)]$  accounts for state occupations, and ensures that transitions only occur between occupied and empty states;  $f$  denotes the occupation number according to Fermi-Dirac statistics. The interaction between carriers in the different states  $\psi_{\mathbf{m}}$  is described by the matrix elements  $M_{1234}$  which are given by

$$|M_{1234}|^2 = |M_{1234}^d - M_{1234}^x|^2 + |M_{1234}^d|^2 + |M_{1234}^x|^2,$$

where  $M_{1234}^d$  ( $M_{1234}^x$ ) are the direct (exchange) screened Coulomb matrix elements:

$$M_{1234}^d = \langle \psi_1 \psi_2 | W | \psi_3 \psi_4 \rangle,$$

$$M_{1234}^x = \langle \psi_1 \psi_2 | W | \psi_4 \psi_3 \rangle.$$

The direct, screened Coulomb interaction (noting that similar arguments hold for the exchange term) may thus be written as

$$M_{1234}^d = e^2 \iint d^3 r d^3 r' \frac{\psi_1^*(\mathbf{r}) \psi_2^*(\mathbf{r}') \psi_3(\mathbf{r}') \psi_4(\mathbf{r}) e^{-\alpha|\mathbf{r}-\mathbf{r}'|}}{4\pi\epsilon_0\epsilon_\infty|\mathbf{r}-\mathbf{r}'|}. \quad (2)$$

The wave functions  $\psi_{\mathbf{m}}$  required for evaluating the above matrix elements are obtained from our TB model. Given that random alloy fluctuations already lead to strong carrier localization effects in (In,Ga)N/GaN QW systems [40,42,45],

the alloy microstructure breaks the symmetry of the system so that the wave vector  $\mathbf{k}$  is no longer a “good” quantum number. Furthermore, when evaluating  $M_{1234}^\lambda$ , with  $\lambda = d$  or  $\lambda = x$  for direct or exchange matrix elements, respectively, we assume a position-independent, and constant, background dielectric function ( $\epsilon_\infty = 5.5$ ) [26,47]. This approximation is often applied in Auger matrix element calculations [48,49].

Following Ref. [26], the inverse screening length  $\alpha$  in Eq. (2) is determined separately for electrons ( $\alpha_e$ ), and holes ( $\alpha_h$ ), by using the Debye-Hückel equation for nondegenerate carriers:  $\alpha_e = \sqrt{\frac{4\pi n e}{\epsilon_0 \epsilon_\infty k_B T}}$ , and for holes  $\alpha_h = \sqrt{\frac{4\pi p e}{\epsilon_0 \epsilon_\infty k_B T}}$ , where  $k_B$  is the Boltzmann constant,  $T$  is the temperature,  $\epsilon_0$  is the vacuum permittivity,  $n$  ( $p$ ) is the electron (hole) carrier density, and  $e$  is the elementary charge. The total inverse free-carrier screening length is then given by  $\alpha^2 = \alpha_e^2 + \alpha_h^2$ .

To calculate  $M_{1234}^\lambda$ , we largely follow the procedure detailed in Ref. [50] to obtain Coulomb matrix elements from TB wave functions. The TB wave functions may be written as

$$\psi_{\mathbf{m}}(\mathbf{r}) = \sum_{\mathbf{R},\sigma} c_{\mathbf{R},\sigma}^{\mathbf{m}} \phi_{\mathbf{R},\sigma}(\mathbf{r}), \quad (3)$$

where  $\phi_{\mathbf{R},\sigma}(\mathbf{r})$  are the localized, atomiclike orbitals,  $\sigma = \{s, p_x, p_y, p_z\}$ , located at a lattice site,  $\mathbf{R}$ , and  $c_{\mathbf{R},\sigma}^{\mathbf{m}}$  are the expansion coefficients of the orbital  $\sigma$  at site  $\mathbf{R}$ . Equipped with this information, the matrix elements are evaluated as

$$M_{1234}^d = \sum_{\mathbf{R},\mathbf{R}'} \sum_{\alpha,\beta} c_{\mathbf{R},\alpha}^{1*} c_{\mathbf{R}',\beta}^{2*} c_{\mathbf{R}',\beta}^3 c_{\mathbf{R},\alpha}^4 W(\mathbf{R} - \mathbf{R}'), \quad (4)$$

with

$$W(\mathbf{R} - \mathbf{R}') = \frac{e^2}{4\pi\epsilon_0\epsilon_\infty} \frac{e^{-\alpha|\mathbf{R}-\mathbf{R}'|}}{|\mathbf{R} - \mathbf{R}'|}, \quad \text{for } \mathbf{R} \neq \mathbf{R}',$$

and

$$W(\mathbf{0}) = \frac{1}{v_{\text{tet}}^2} \int_{\text{tet}} \frac{e^2}{4\pi\epsilon_0} \frac{1}{|\mathbf{r} - \mathbf{r}'|} \approx W_0, \quad \text{when } \mathbf{R} = \mathbf{R}'.$$

The on-site energy,  $W_0$ , can be calculated quasianalytically, as described in Ref. [50], and in more detail in Appendix A, by integrating over a sphere of volume equal to that of the local tetrahedron formed by the nearest neighbors of an atom in the wurtzite unit cell. This approximation is widely used in determining the Coulomb matrix elements from TB wave functions [50–53], building on the finding that in general the dominant contributions to the Coulomb matrix elements stem from the long-ranged part; therefore, the localized orbitals,  $\phi_{\mathbf{R},\sigma}(\mathbf{r})$ , underlying the TB model can be treated, in a first approximation, as point charges, and thus the explicit structure of the localized orbitals is of secondary importance [50,51,54,55]. The impact of the on-site Coulomb energy,  $W_0$ , on the Auger rate is also discussed in more detail in Appendix A.

Finally, and following previous work on calculating the Auger rate in III-N materials [32,56], the fourth state (4) in Eq. (1), into which the carriers can scatter, is always unoccupied. In addition to the preevaluated 100 electron and hole states discussed below, we have also performed further calculations to investigate the impact of this energetically higher- and/or lower-lying (fourth) state on the results. First, our calculations revealed a continuum of states (energy separation  $\leq 0.5$  meV) in the range of the magnitude of the band gap

above (below) the conduction (valence) “band” edge. Testing Auger rates with different “final” fourth states from this continuum revealed that the specific choice of the fourth state was of secondary importance to the results when compared to the spread in values introduced by alloy fluctuations. Thus, a precalculated continuum state is used for each In content. Additionally, despite the existence of such a continuum of states, the energy conservation requirement in the Auger rate calculation, given by the  $\delta$  function in Eq. (1), is never exactly numerically satisfied. Therefore, the  $\delta$  function was replaced by a Gaussian function and the impact of the broadening parameter on the results was tested. These investigations showed that a broadening parameter of 1 meV is sufficient to achieve converged results; i.e., choosing a smaller value did not change the results.

Equipped with this information, we obtain the Auger coefficients from the Auger rate,  $R$ , using  $C = R/(Vn^3)$ . Here,  $V$  is the volume of the well, and  $n$  is the carrier density; for all calculations we have assumed that  $p = n$ , i.e., that the density of holes is equal to that of electrons, as is done in other works [26,30,37].

### III. RESULTS AND DISCUSSION

Using the framework detailed above, we have investigated the *alloy-enhanced* electron-electron-hole,  $C_{eeh}$ , and hole-hole-electron,  $C_{hhe}$ , Auger coefficients; the total Auger coefficient,  $C_{\text{tot}}$ , was then obtained via  $C_{\text{tot}} = C_{eeh} + C_{hhe}$ . Phonon-assisted Auger processes were not considered since the DFT calculations in Ref. [26] show that (i) Auger processes can be significantly enhanced by alloy fluctuations and that (ii) in the band-gap range of approximately 1.9–3.0 eV, which corresponds to the ground-state transition energies of the QW structures studied here, contributions from phonon-assisted Auger processes are smaller compared to the alloy-enhanced scattering effects. Thus, it can be expected that alloy-enhanced Auger recombination is the dominant contribution in the (In,Ga)N-based QWs investigated here.

Following Ref. [33], which has adapted the experimental data from Ref. [24], our calculations have been carried out at a fixed carrier density of  $n_{3D} = 3.8 \times 10^{18} \text{ cm}^{-3}$  (corresponding to a sheet carrier density of  $n_{2D} \approx 1.0 \times 10^{12} \text{ cm}^{-2}$ ). For this relatively low carrier density we have performed initial, self-consistent, one-dimensional Schrödinger-Poisson calculations which show that the screening of the built-in field (i.e., its reduction) is of secondary importance. This approximation is supported by the experimental and theoretical works of Refs. [20,57,58]. Furthermore, we have tested several configurations with such a reduced (i.e., screened) field and found that the screening of the intrinsic (spontaneous and piezoelectric) built-in field only affected the ground and excited electron and hole states by less than 24 meV (most often by only  $\approx 3$ –5 meV). However, the screening of the built-in field may affect states near the band edges (e.g., localized hole states) differently to energetically higher-lying states, which may exhibit a more delocalized character (see Ref. [59] for more details on the distribution of localized, “semilocalized,” and delocalized states). To analyze this situation in more detail, while taking into account the numerical expense of these calculations, we have evaluated the Auger coefficient

at a temperature of 300 K for one (randomly selected) configuration with and without the built-in field screening. In such a higher-temperature calculation not only energetically lower-lying states but also excited states will become relevant, which provides insight into the impact of the screening on the energetically higher-lying states (both hole and electron states). This study revealed that the results in the presence and absence of the built-in field screening differed by less than 8%. Overall, this difference is regarded as not only smaller than the uncertainties in some of the material parameters entering the calculations (e.g., the dielectric constants), but also smaller than variations introduced by the alloy microstructure. Furthermore, the calculations by David *et al.* [25,60] show that the Coulomb enhancement of the radiative recombination rate is of secondary importance for a carrier density of  $n_{3D} \approx 3 \times 10^{18} \text{ cm}^{-3}$ . Thus, we directly use the TB wave functions (without Coulomb enhancement or built-in field screening effects) when calculating the  $C$  and  $B$  coefficients; future studies will focus on the impact of the carrier density on the results.

To this end we have employed the TB model described above to calculate 100 electron and 100 hole states for ten different microscopic alloy configurations for  $c$ -plane (In,Ga)N/GaN QWs with 10%, 15%, and 25% In content. Using this large number of precalculated states, we are in the position to study the impact of temperature effects on the Auger rate at a fixed carrier density of  $n_{3D} = 3.8 \times 10^{18} \text{ cm}^{-3}$ . We note that while the wave functions entering Eq. (2) are directly taken from the TB model, a carrier-density-dependent Debye screening length for the Coulomb interaction between the carriers has been taken into account (see above). Moreover, our previous studies [61] indicate that a carrier density of  $n_{3D} = 3.8 \times 10^{18} \text{ cm}^{-3}$  is not large enough to saturate the localized hole states in (In,Ga)N-based QWs with 10%, 15%, and 25% In; electrons are far less strongly affected by alloy fluctuations and exhibit a more delocalized wave-function character [59]. Therefore, one can still expect that carrier localization effects will impact both the Auger and also the radiative recombination processes in the systems studied here.

Equipped with all this information, Figs. 1(a) and 1(b) display the evolution of the alloy-enhanced  $C_{eeh}$  and  $C_{hhe}$  Auger coefficients, respectively, as a function of temperature,  $T$ , for the different In contents considered; the carrier density is fixed at  $n_{3D} = 3.8 \times 10^{18} \text{ cm}^{-3}$ . The data are averaged over the ten different microscopic configurations per In content; error bars indicate the *maximum* and *minimum* values of  $C_{\lambda}$  ( $\lambda = \{eeh, hhe\}$ ) at a given  $T$ . The reason for using the minimum and maximum values is to highlight that the magnitude of the predicted coefficients may strongly depend on the alloy microstructure. Therefore, using just a single alloy configuration to evaluate Auger coefficients may over- or underestimate these coefficients. Overall, we observe that the  $C_{eeh}$  coefficients increase with increasing  $T$  [Fig. 1(a)], while the  $C_{hhe}$  coefficients show a weak  $T$  dependence or (slight) decrease [Fig. 1(b)]. Furthermore, Figs. 1(a) and 1(b) reveal that, independent of temperature and In content,  $C_{hhe}$  is greater than  $C_{eeh}$  [note the different scales in Figs. 1(a) and 1(b)].

To gain further insight into the relative contributions from  $C_{eeh}$  and  $C_{hhe}$  to  $C_{\text{tot}}$ , a detailed breakdown is presented

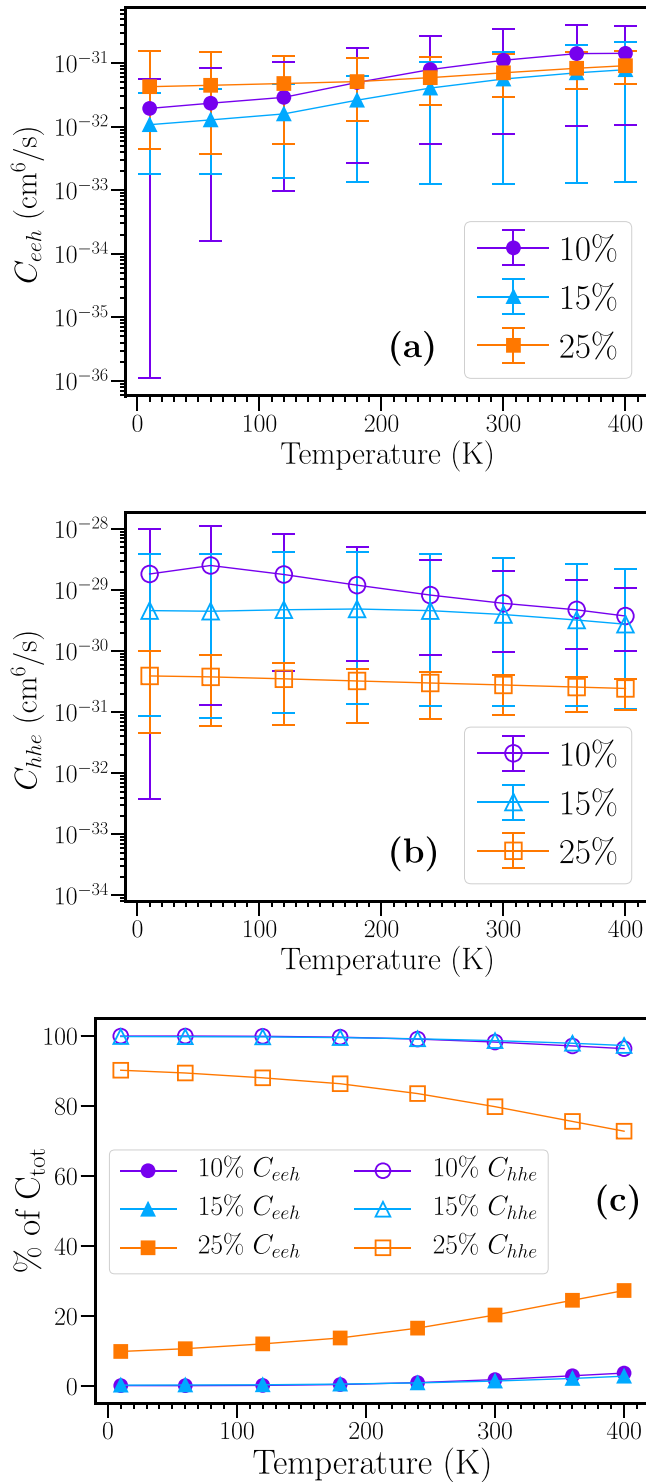


FIG. 1. (a) Electron-electron-hole,  $C_{eeh}$ , and (b) hole-hole-electron,  $C_{hhe}$ , Auger coefficients as a function of the temperature,  $T$ , for *c*-plane (In,Ga)N/GaN quantum wells with different In contents (10%, 15%, and 25%). The data, averaged over ten microscopic alloy configurations, are given by the solid ( $C_{eeh}$ ) and open ( $C_{hhe}$ ) symbols; error bars indicate maximum and minimum values of  $C_\lambda$  ( $\lambda = \{eeh, hhe\}$ ) at a given temperature, across the ten configurations. The calculations have been carried out at a fixed carrier density of  $n_{3D} = 3.8 \times 10^{18} \text{ cm}^{-3}$ . (c) Percentage breakdown of the contribution from  $C_{eeh}$  and  $C_{hhe}$  to the total Auger coefficient,  $C_{\text{tot}}$ .

in Fig. 1(c). As already discussed above, in general, the contribution from  $C_{eeh}$  to  $C_{\text{tot}}$  is smaller relative to the contribution from  $C_{hhe}$ , for all considered In contents; this finding is consistent with previous theoretical studies [26,32]. However, Fig. 1(c) reveals that the relative contribution depends on the In content. In the 10% and 15% In cases,  $C_{hhe}$  makes up  $\gtrsim 99\%$  of  $C_{\text{tot}}$ , independent of  $T$ ; this is in contrast to the 25% In case, where the contribution from  $C_{hhe}$  reduces to around 90% at low temperatures and as low as approximately 75% at higher temperatures. We attribute this effect to the following factors: as several works have already shown [32,45,59], hole wave functions are strongly affected by (random) alloy fluctuations. Thus, the local potential fluctuations mainly affect the hole-hole wave-function overlaps (i.e., the spatial in-plane separation between the states). However, the electron wave functions exhibit a more delocalized character compared to the holes. Now, with increasing In content the intrinsic electrostatic built-in field increases, which leads to stronger confinement of the electron and hole wave functions at the QW interfaces. On the one hand, this reduces the electron-hole wave-function overlap in the out-of-plane direction (along the wurtzite *c* axis), and we attribute the observed overall reduction in Auger coefficient with increasing In content to the reduction in the electron-hole wave-function overlap (also see discussion below). On the other hand, given the more delocalized character of the electron wave functions, the electron-electron wave-function overlap, which is relevant to the Auger rate of the *e-e-h* process, should be more strongly affected by the built-in field increase than the hole-hole wave-function overlap, which is relevant to the *h-h-e* Auger process, and which is mainly affected by alloy-induced localization effects (e.g., spatial separation in the growth plane or wave functions localized in the same potential pocket).

This is supported by our calculations on (In,Ga)N/GaN QWs as a function of the electric field strength [62]: the hole wave functions, even at a “zero-field” value, still show strong localization effects while the electron wave functions, initially strongly localized by well width fluctuations, become spread out over the full QW width in the case of “zero field.” A similar situation is found in nonpolar (In,Ga)N-based QWs [63]. This already indicates that electron and hole wave functions are affected differently by changes in the internal built-in field strength. The increase in electron-electron wave-function overlap, due to the increased built-in field at higher In contents, may be even more pronounced in the presence of well width fluctuations at the upper QW interface [59,62]. As a consequence, one may expect that the relative contribution from  $C_{eeh}$  to  $C_{\text{tot}}$  increases with increasing In content, as is reflected in our data. However, the overall magnitude of the Auger coefficient decreases with increasing In content, as we will discuss further below. We also note that the phenomenon of an increasing  $C_{eeh}$  contribution with increasing In content would not be present in a bulk system due to the absence of any macroscopic built-in field and, thus, may not arise in any DFT-based calculation on bulk systems.

Having discussed the relative contributions from  $C_{eeh}$  and  $C_{hhe}$  to the total Auger coefficient,  $C_{\text{tot}}$ , and how they change with temperature and alloy composition, in the next step we focus on the interplay of the alloy microstructure, temperature, and In content. Starting with  $C_{hhe}$ , Fig. 1(b) shows that

the Auger coefficient decreases with increasing In content as one may expect due to the increasing (piezoelectric) built-in field and the related strong hole localization effects. We note, however, that there is a large “spread” in the Auger coefficients due to the alloy microstructure; we will come back to this aspect below.

Turning to  $C_{eeh}$ , Fig. 1(a), we find that on average the results for 10% and 15% In show a similar trend: with increasing In content  $C_{eeh}$  decreases. But, at low temperatures the  $C_{eeh}$  coefficient for the 25% In systems is larger in magnitude compared to both the 10% and 15% In systems; however, due to its much weaker temperature dependence at higher temperatures, the  $C_{eeh}$  coefficients of the 15% and 25% In cases are on average basically identical, while the 10% In case is slightly larger. We attribute the higher  $C_{eeh}$  for 25% In at low temperatures to stronger localization of the electron wave functions at the QW interfaces (i.e., confinement by well width fluctuations), as already discussed above and seen in the electronic structure calculations in Ref. [59].

We now turn to the impact of the alloy microstructure and temperature on the results. The error bars in Figs. 1(a) and 1(b) give insight into the importance of the alloy microstructure for the Auger coefficients. We observe that with increasing  $T$  the “spread” in both  $C_{eeh}$  and  $C_{hhe}$  coefficients, in general, decreases. We attribute this to the effect that at low temperatures only states near the conduction and valence “band” edges are populated by the carriers. These are strongly localized states [59] and the wave-function overlap between them may strongly depend on the alloy microstructure. As the temperature is increased, the carriers start to populate states where the corresponding wave functions are more delocalized compared to the “band” edge states. This has three consequences: (i) in general, the wave-function overlap between electron and hole wave functions along the growth direction is (slightly) increased; (ii) in contrast, potential contributions from locally strongly overlapping hole wave functions due to carrier localization effects are reduced; and (iii) for these more delocalized states the alloy fluctuations present a weaker perturbation and the wave-function overlap is less dependent on the alloy microstructure. As shown in Fig. 1, consequences (i) and (ii) lead to opposite effects, with  $C_{eeh}$  slightly increasing with increasing temperature (at least for 10% and 15% In) while  $C_{hhe}$  (slightly) decreases with increasing temperature. Furthermore, consequence (iii) results in the situation that the importance of the alloy microstructure is reduced with increasing temperature and thus the “spread” in both the  $C_{eeh}$  and  $C_{hhe}$  coefficients decreases.

However, for the 15% In QWs we find that even at higher temperatures there is still a noticeable spread in the Auger coefficient values. As previously shown [59], the interplay of the built-in field, structural inhomogeneities, and the alloy microstructure can affect the wave-function localization. As discussed in more detail in Appendix B, when breaking the 15% In QW  $C_{hhe}$  coefficient down into the individual contributions, we find eight configurations which exhibit very similar  $C_{hhe}$  values while two configurations result in much higher values. Furthermore, our analysis shows that these large coefficients are linked to very high valence “band” (hole) energies. This is indicative of strong hole wave-function localization effects. Our finding here may also tie in with

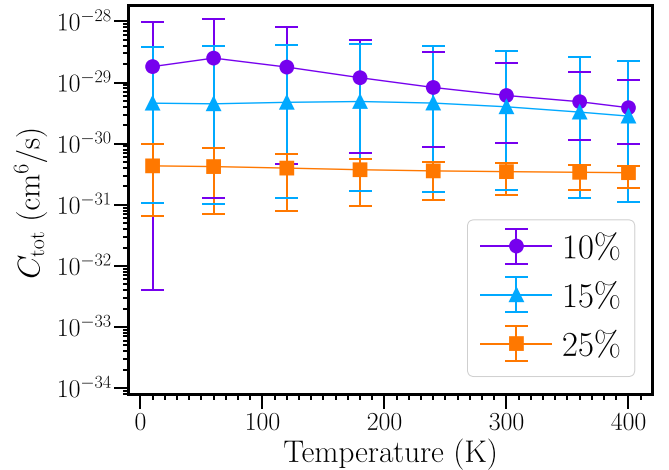


FIG. 2. Total Auger coefficient,  $C_{tot}$ , as a function of the temperature,  $T$ , for  $c$ -plane (In,Ga)N/GaN quantum wells with different In contents (10%, 15%, and 25%). The data, averaged over ten microscopic configurations, are given by the solid symbols; error bars indicate maximum and minimum values of  $C_{tot}$  at a given temperature, across the ten configurations. The calculations have been carried out at a fixed carrier density of  $n_{3D} = 3.8 \times 10^{18} \text{ cm}^{-3}$ .

recent studies of trap-assisted Auger recombination effects, where the presence of traps (localized states within the band gap) may lead to a significant enhancement of the Auger effect [64,65].

Having discussed the temperature dependence of, and the impact of the alloy microstructure on,  $C_{eeh}$  and  $C_{hhe}$  in detail, we now turn to analyzing the *total* Auger coefficient,  $C_{tot} = C_{eeh} + C_{hhe}$ . Figure 2 displays  $C_{tot}$  as a function of temperature for the three different In contents considered. In general,  $C_{tot}$  reflects the features of  $C_{hhe}$  in that (i)  $C_{tot}$  decreases with increasing In content, independent of the temperature, (ii) the impact of the alloy microstructure, and thus the spread in the  $C_{tot}$  values, in general decreases with increasing  $T$ , and (iii) the Auger coefficient shows a weak  $T$  dependence, or a (slight) decrease with increasing  $T$ .

As already highlighted in the Introduction, there have been multiple theoretical studies focusing on the Auger coefficient in (In,Ga)N/GaN QWs. While these studies come in different flavors (e.g., effective-mass models plus scaling of the bulk Auger coefficients, eight-band  $\mathbf{k} \cdot \mathbf{p}$  models, and full-zone  $\mathbf{k} \cdot \mathbf{p}$  models) they basically all rely on continuum-based electronic structure models. Thus, most of these models neglect alloy fluctuations. Looking at the results from some of these theoretical models and approaches, Bertazzi *et al.* [16] found an upper bound estimate for the Auger coefficient in an  $\text{In}_{0.25}\text{Ga}_{0.75}\text{N}/\text{GaN}$  QW of  $5 \times 10^{-31} \text{ cm}^6 \text{ s}^{-1}$  using a full-zone  $\mathbf{k} \cdot \mathbf{p}$  model. While this number is similar to our calculated values, the model in Ref. [16] neglects not only polarization fields but carrier localization effects too. The polarization fields may reduce the Auger coefficients, while alloy fluctuations should increase the Auger coefficients, since, for instance,  $k$ -selection rules are removed. This was already highlighted by Jones *et al.* [32] where, by using a three-dimensional (3D) effective-mass model in conjunction with scaled bulk Auger coefficients, they showed that includ-

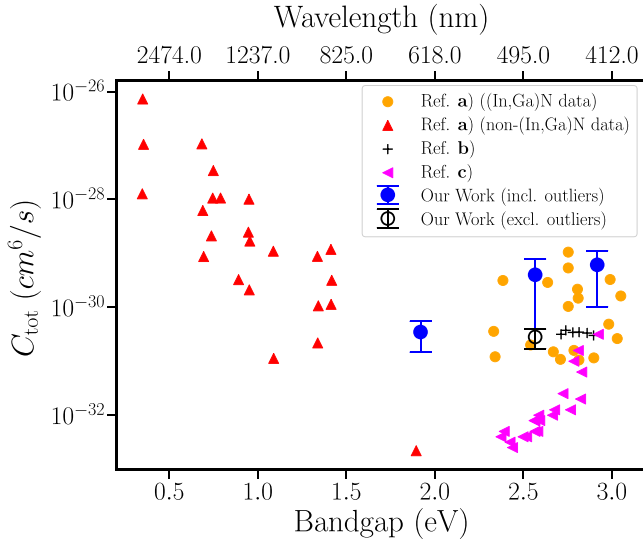


FIG. 3. Comparison of calculated and measured Auger coefficients ( $C_{\text{tot}}$ ) as a function of (effective) band gap and emission wavelength. Data from several literature sources are included. **a** = Ref. [21], **b** = Ref. [22], **c** = Ref. [37].

ing alloy fluctuations led to an enhancement of the Auger coefficients compared to systems without alloy fluctuations. For a  $c$ -plane  $\text{In}_{0.25}\text{Ga}_{0.75}\text{N}/\text{GaN}$  QW, Jones *et al.* [32] report total Auger coefficients of approximately  $7 \times 10^{-33} \text{ cm}^6 \text{ s}^{-1}$ , at 300 K and a carrier density of  $n_{3D} = 10^{19} \text{ cm}^{-3}$ , when alloy fluctuations are taken into account. This value is smaller than the value reported here, but as we have recently shown, effective-mass models can significantly underestimate carrier localization effects. Thus, if alloy fluctuations lead to an increase in the Auger coefficient, stronger carrier localization may increase the values reported by Jones *et al.* significantly.

A direct comparison of our calculated Auger coefficients with experiment, in terms of the In content evolution, is difficult since, for instance, in Refs. [24,66] only emission wavelengths, or classifications such as “green” or “blue” emitting wells, are reported and these different wavelength regimes may be realized by different alloy and well width combinations. However, to gain some first insights into how our calculated values compare with literature data, Fig. 3 compares our calculated total Auger coefficients at a temperature of 300 K with literature data, both from experiment and theory, as a function of the (effective) band gap or emission wavelength. To make this comparison we have used the expression from Ref. [67],

$$E_g(T) = E_g(0) - \frac{\alpha T^2}{\beta + T} - \frac{\sigma^2}{k_B T^2},$$

to obtain the (effective) band gap for our QW structures at 300 K. The low-temperature band gap,  $E_g(0)$ , is found by calculating the TB single-particle electron-hole ground-state transition energy averaged over the ten microscopic configurations considered. The values used for  $\alpha$ ,  $\beta$ , and  $\sigma$  are taken from Ref. [29].

As already seen in other work [21], Fig. 3 indicates the unconventional plateau or increase of  $C_{\text{tot}}$  with increasing

(effective) band gap in (In,Ga)N systems, when compared to the sharp decline in  $C_{\text{tot}}$  for other material systems with increasing band gap; furthermore, our calculated values are within the large spread of literature values.

It is now also interesting to study the impact of the “outliers,” mentioned above for the 15% In case, on the results. When including all ten microscopic configurations in the averaging procedure (blue solid circle), our calculations indicate that the Auger coefficient increases with increasing band gap. Although the magnitudes are different, a similar dependence of the Auger coefficient on the (effective) band-gap value is observed in the experimental studies from Ref. [37]. On the other hand, when excluding the two “outlier” configurations in the 15% In results (averaging over eight alloy configurations), we find that the Auger coefficient is, in terms of magnitude, very similar to the 25% In case. As a consequence, our calculated Auger coefficients only vary weakly in the energy range of  $\approx 1.9 \text{ eV}$  ( $\approx 644 \text{ nm}$  at 25% In) to  $\approx 2.6 \text{ eV}$  ( $\approx 482 \text{ nm}$  at 15% In); a similar behavior was found in the experimental studies of, for instance, Schiavon *et al.* [66]. However, we find that when going to larger effective band gaps (i.e.,  $\approx 2.9 \text{ eV}/424 \text{ nm}$  at 10% In) the Auger coefficient increases, while in Ref. [66] the coefficient is largely constant or may only be slightly increasing beyond 2.6 eV. Overall, our analysis highlights that the alloy microstructure (for instance, “trap states”) can play an important role in the magnitude of the Auger coefficient and thus further studies are required to gain insight into this question.

Continuing our analysis of the temperature dependence of the recombination rates and to provide further insight into the thermal droop phenomenon in (In,Ga)N-based QW systems, we now present the previously studied temperature dependence of the radiative recombination (expressed by the  $B$  coefficient) alongside the nonradiative Auger recombination rate; special emphasis is placed on the competition between these two rates. The calculation of  $B$ , performed on the same systems studied here, is discussed in more detail in Ref. [28]. We highlight two important aspects. First, the observed strong decrease in  $B$  with increasing In content can be attributed to the increase in the strain-dependent piezoelectric polarization field. Second, at low temperatures only states near the band edge are populated. These states are strongly localized, especially in the case of the holes [59]. With increasing temperature, excited states may be populated, which results in an increase in the overlap of the electron and hole wave functions. This, in turn, can lead to the unusual behavior that the  $B$  coefficient increases with increasing temperature  $T$ ; such an effect has also been observed in the experimental studies by Nippert *et al.* [24]. Figure 4 displays  $B$ ,  $C_{\text{tot}}$ , and the  $B/C_{\text{tot}}$  ratio as a function of the temperature (above 300 K) for the three different In contents considered; the  $B/C_{\text{tot}}$  ratio has been *normalized* to the respective values at 300 K. We stress that the carrier density is fixed and that we present the *relative* change in  $B/C_{\text{tot}}$  to gain insight into the *temperature-dependent* competition between radiative and Auger recombination. As a result, Fig. 4 will be identical when plotting the *relative* change of, for instance,  $B/(C_{\text{tot}}n_{3D})$ . The data show that  $B$  increases slightly while  $C_{\text{tot}}$  varies weakly with  $T$  in the 25% In case, or decreases with increasing temperature in the 10% and 15% In cases.

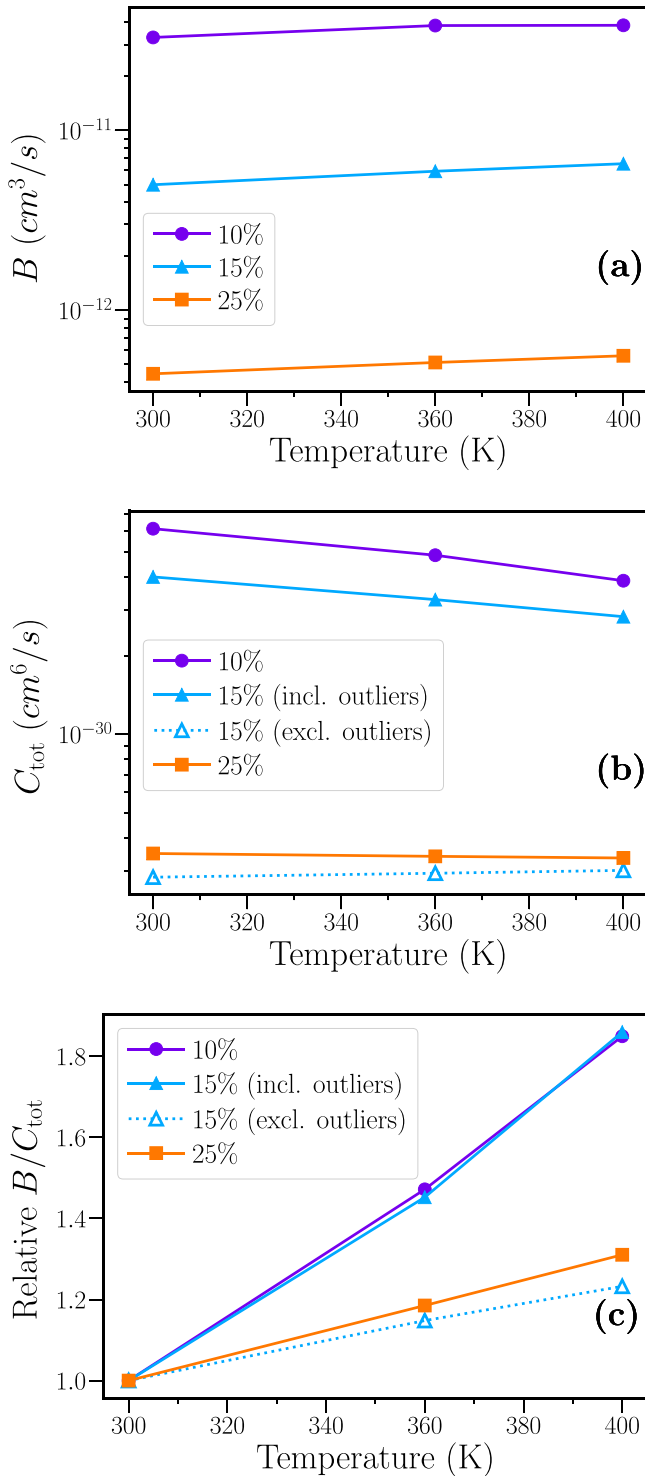


FIG. 4. (a) Radiative coefficient  $B$ , (b) total nonradiative Auger coefficient  $C_{\text{tot}}$ , and (c) ratio of these coefficient  $B/C_{\text{tot}}$ , relative to  $B/C_{\text{tot}}$  at 300 K, as a function of temperature (above 300 K) for 10%, 15%, and 25% indium in the well. The carrier density is fixed at  $n_{3D} = 3.8 \times 10^{18} \text{ cm}^{-3}$ .

Looking at the  $B/C_{\text{tot}}$  ratio, we always find values  $> 1$ , noting again that this value is relative to the value at 300 K, which would indicate that the “efficiency” of the systems should increase with increasing temperature, even though, overall,

the absolute magnitude of the  $B/C_{\text{tot}}$  ratio is decreasing as In content increases (further discussion below). We note that the smaller rate of increase of the  $B/C_{\text{tot}}$  ratio for the 25% case is primarily explained by the weaker  $T$  dependence of the 25% total Auger rate, in contrast to the decreasing rates for 10% and 15% In, at least when taking all alloy configurations for the 15% In case into account. Excluding the two extreme configurations of the 15% In case from the calculations, the situation slightly changes: while the  $B/C_{\text{tot}}$  ratio is still larger than 1, the weaker  $T$  dependence of  $C_{\text{tot}}$  in the 15% In case leads to a  $B/C_{\text{tot}}$  ratio similar to the 25% In system.

Overall, given our finding of an increase of  $B/C_{\text{tot}}$  with temperature, one could expect that the likelihood of a photon being produced during a recombination event would increase relative to the likelihood of the carrier undergoing a nonradiative Auger process. Thus, our results indicate that the alloy-enhanced Auger processes studied here should not lead to a deterioration of device efficiency as temperature increases. Therefore, we conclude that the experimentally observed thermal droop [17] is not caused by alloy-enhanced Auger recombination, and other nonradiative recombination processes, for instance defect-assisted processes, are more likely to be its origin.

Having analyzed the impact of temperature on the radiative recombination rate, as well as its impact on the nonradiative Auger recombination rate, and the competition between the two rates, we now turn to investigate the impact of In content on the recombination rates and their competition. We note again that with increasing In content the strain-dependent piezoelectric field increases, which in turn leads to a spatial separation of electron and hole wave functions and will thus modify the electronic structure of the wells. Figures 5(a) and 5(b) show the change of  $B$ ,  $C_{\text{tot}}$ , and  $B/C_{\text{tot}}$  with increasing In content at a fixed temperature of 300 K and fixed carrier density. The data are shown *relative* to the 10% In system; for the 15% In QW system we present the results when excluding [Fig. 5(a)] and including [Fig. 5(b)] the two “outlier” alloy configurations. Looking at the results when excluding the outliers first [Fig. 5(a)], we find that when going from 10% to 15% In content,  $C_{\text{tot}}$  drops faster than  $B$ , resulting in an increase of the  $B/C_{\text{tot}}$  ratio. When increasing the In content further to 25%, we find that  $B$  continues to drop quickly while  $C_{\text{tot}}$  shows only a weak In content dependence, slightly increasing by approximately 10%. As a consequence, the  $B/C_{\text{tot}}$  ratio drops, but this drop can be attributed to the reduction of  $B$  when increasing the In content from 15% to 25%, and is not due to a significant increase in  $C_{\text{tot}}$ .

Turning to our results when including the outliers in the 15% In system, Fig. 5(b), we find that when increasing the In content from 10% to 15%, the  $B$  coefficient decreases more quickly than the nonradiative Auger coefficient,  $C_{\text{tot}}$ . However, when increasing the In content from 15% to 25%,  $B$  and  $C_{\text{tot}}$  decrease at a similar rate. This is reflected in the  $B/C_{\text{tot}}$  ratio in Fig. 5(b) by its approximately flat slope between 15% and 25% In.

Overall, both investigations indicate that the “green gap” [29], i.e., the reduction of IQE in (In,Ga)N-based light emitters operating in the green to yellow spectral range, and thus at higher In contents (i.e.,  $> 15\%$ ), may not be caused by *alloy-enhanced* Auger recombination effects, since Fig. 5 indicates



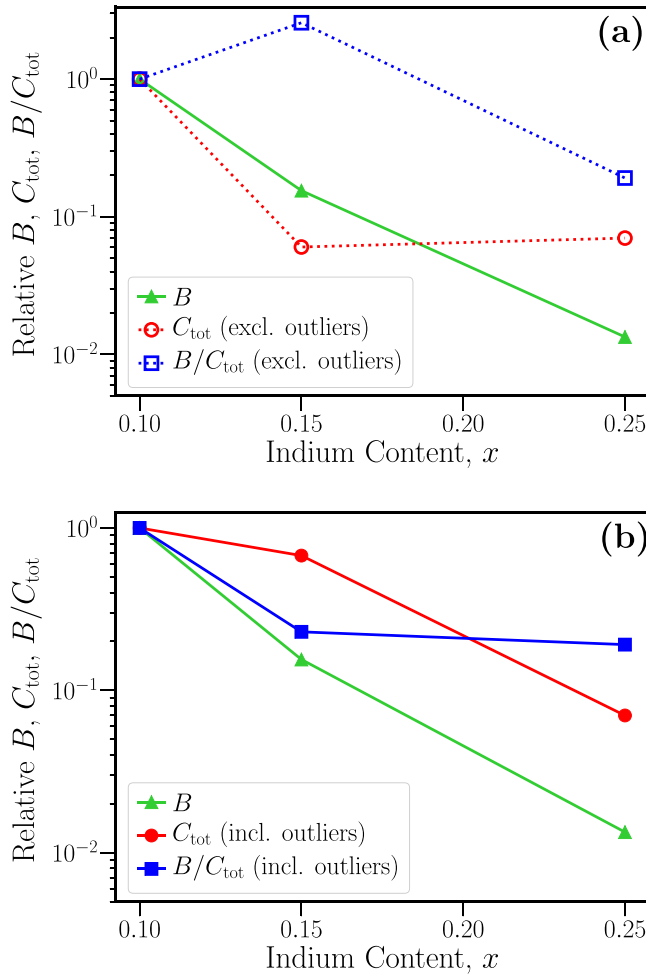


FIG. 5. Radiative coefficient  $B$ , nonradiative Auger coefficient  $C_{\text{tot}}$ , and ratio of these coefficients  $B/C_{\text{tot}}$ , as a function of the indium content  $x$ , when (a) excluding and (b) including outlier configurations. The data are shown relative to their respective values at 10% In. All data are given at a temperature of 300K and a fixed carrier density of  $n_{3D} = 3.8 \times 10^{18} \text{ cm}^{-3}$ .

that it is the reduction of  $B$  and not an increase in  $C$  that determines the composition dependence of  $B/C_{\text{tot}}$ . In other words, the alloy-enhanced Auger recombination may not present an intrinsic roadblock to achieving efficient recombination in the green to yellow range. Thus, in addition to the reduction of the radiative recombination rate when increasing the In content, other factors, such as an increasing defect density and the connected nonradiative recombination processes (e.g., *trap-assisted* Auger recombination [64] or Shockley-Read-Hall recombination [68]) in higher In content samples, are more likely to be responsible for the green gap problem. This suggests that by reducing defect densities and thus the connected nonradiative recombination in high In content systems, there may be a way forward to close the green gap. David *et al.* [64] comes to a similar conclusion and suggests that reducing the (point) defect density could close the green gap.

#### IV. CONCLUSION

In this work we presented an atomistic theoretical framework to describe the nonradiative Auger recombination rate in  $c$ -plane (In,Ga)N/GaN quantum wells. The model was employed to study the competition between (nonradiative) Auger and radiative recombination processes in (In,Ga)N-based systems. In our investigations, while keeping the carrier density fixed, we paid special attention to the impact of temperature, In content, and alloy microstructure on the Auger rate. Our calculations revealed that electron-electron-hole Auger recombination shows a weak temperature dependence, or increases slightly, with increasing temperature. In comparison, the hole-hole-electron Auger rate shows a weak temperature dependence, or a (slight) decrease, with increasing temperature. Our studies also revealed that the relative contributions from electron-electron-hole and hole-hole-electron Auger rates to the total rate change with In content. While, in general, the hole-hole-electron Auger recombination is the dominant contribution, the relative importance of the electron-electron-hole rate increases with increasing In content, and temperature.

Our investigations also show that at temperatures greater than 300 K the radiative recombination rate slightly increases while the total Auger recombination rate (slightly) decreases; this finding would indicate a positive impact of increasing temperature on device efficiency. However, this stands in contrast to experimental studies which show that the device efficiency decreases with increasing temperature in this temperature range. Therefore, we conclude that the alloy-enhanced Auger recombination process is not responsible for this *thermal* droop observed in  $c$ -plane (In,Ga)N/GaN quantum wells, and other factors, such as carrier transport, defects, and defect-assisted Auger recombination, are more likely to explain the experimentally observed droop effect.

#### ACKNOWLEDGMENTS

The authors acknowledge the financial support from Science Foundation Ireland (SFI) and the Sustainable Energy Authority of Ireland under Grants No. 17/CDA/4789 and No. 12/RC/2276 P2, and the University of Michigan Blue Sky Research Program. Furthermore, computing resources provided by SFI to the Tyndall National Institute, and by the SFI and Higher Education Authority (HEA) funded Irish Centre for High End Computing (ICHEC) are acknowledged.

#### APPENDIX A: DISCUSSION OF ON-SITE ENERGIES

In this section we provide further information on the Coulomb matrix element calculations and the impact of the on-site energy,  $W_0$ , on the Auger rates. In the following we focus our attention on the general form of the Coulomb matrix elements,

$$M = \frac{e^2}{4\pi\epsilon_0\epsilon_r} \iint d^3\tilde{r}' d^3\tilde{r} \frac{\psi_1^*(\tilde{r}')\psi_2(\tilde{r}')\psi_3^*(\tilde{r})\psi_4(\tilde{r})}{|\tilde{r} - \tilde{r}'|}. \quad (\text{A1})$$

Here, each  $\psi(\tilde{r})$  is a TB wave function, which are given by Eq. (3), i.e., by linear combinations of localized, atomiclike orbitals,  $\phi_{\mathbf{R},\sigma}(\tilde{r})$ ,  $\sigma = \{s, p_x, p_y, p_z\}$ , located at the lattice sites,  $\mathbf{R}$ . In the following we make the two-center approxi-

mation discussed in detail in Ref. [50], so that the Coulomb matrix element,  $M$ , becomes

$$M \approx \frac{e^2}{4\pi\epsilon_0\epsilon_r} \sum_{\mathbf{R}, \mathbf{R}' \alpha, \beta, \gamma, \delta} c_{\mathbf{R}'\alpha}^* c_{\mathbf{R}'\delta} c_{\mathbf{R}\beta}^* c_{\mathbf{R}\gamma} \\ \times \iint d^3r' d^3r \frac{\phi_{\mathbf{R}'\alpha}^*(\mathbf{r}') \phi_{\mathbf{R}'\delta}(\mathbf{r}') \phi_{\mathbf{R}\beta}^*(\mathbf{r}) \phi_{\mathbf{R}\gamma}(\mathbf{r})}{|\mathbf{R} + \mathbf{r} - \mathbf{R}' - \mathbf{r}'|}.$$

Here, we have decomposed the positions  $\tilde{\mathbf{r}}$  and  $\tilde{\mathbf{r}}'$  into the positions  $\mathbf{R}$  and  $\mathbf{R}'$  of the lattice sites and the positions  $\mathbf{r}$  and  $\mathbf{r}'$  inside the local tetrahedron of the lattice site. Due to the localized nature of the atomiclike orbitals  $\phi_{\mathbf{R},\sigma}(\mathbf{r})$ , when the lattice sites at which the orbitals are localized are far apart, the exact structure of these  $s$ - and  $p$ -like orbitals is of secondary importance. In doing so, one ends up with the approximation given in Eq. (4).

However, when the situation  $\mathbf{R} = \mathbf{R}'$  arises, this on-site contribution needs to be treated carefully. In principle, the specific form of the atomiclike basis states needs to be known.

To this end, we now employ the often used approach [69,70] to approximate  $\phi_{\mathbf{R},\sigma}(\mathbf{r})$  via Slater orbitals [71], which can be written, in general, as

$$\phi_n(\mathbf{r}) = R_n(r)Y_n(\theta, \phi), \quad (\text{A2})$$

where the index  $n$  denotes the orbital type,  $Y_n(\theta, \phi)$  are spherical harmonics, and  $R_n(r) = Dr^a e^{-br}$  are the radial parts; the constants  $a$  and  $b$  are given by Slater's rules [71] and  $D$  is a normalization constant. Given that we are evaluating on-site energies, and without loss of generality, we assume  $\mathbf{R} = \mathbf{R}' = \mathbf{0}$ . Equipped with these orbitals, in this second step, we expand the Coulomb potential in spherical harmonics [72]:

$$\frac{1}{|\mathbf{r} - \mathbf{r}'|} = \sum_{l=0}^{\infty} \frac{4\pi}{2l+1} \frac{r_{<}^l}{r_{>}^{l+1}} \sum_{m=-l}^l Y_{lm}^*(\mathbf{r}') Y_{lm}(\mathbf{r}).$$

Here,  $r_>$  ( $r_<$ ) is the length of the larger (smaller) of the vectors  $\mathbf{r}$  and  $\mathbf{r}'$ . Using the above, and Eq. (3), the Coulomb matrix element  $M$  becomes, for the case of  $\mathbf{R} = \mathbf{R}' = \mathbf{0}$ ,

$$M = \frac{e^2}{4\pi\epsilon_0} \sum_{l,\{n\}} c_{n_1}^* c_{n_2} c_{n_3}^* c_{n_4} \int dr' \int dr r'^2 R_{n_1}(r') R_{n_2}(r') r^2 R_{n_3}(r) R_{n_4}(r) \frac{r_{<}^l}{r_{>}^{l+1}} \frac{4\pi}{2l+1} \sum_{m=-l}^l K_{n_1, n_2, l, m} K_{n_3, n_4, l, m}. \quad (\text{A3})$$

The coefficients  $K_{n, n', l, m}$  are the so-called Gaunt coefficients [73]. We define now

$$M = \sum_{\{n\}} c_{n_1}^* c_{n_2} c_{n_3}^* c_{n_4} \sum_l \mathcal{K}_{n_1, \dots, n_4}^l \times \mathcal{I}_{n_1, \dots, n_4}^l = \sum_{\{n\}} c_{n_1}^* c_{n_2} c_{n_3}^* c_{n_4} W_0$$

with

$$\mathcal{K}_{n_1, \dots, n_4}^l = \frac{4\pi}{2l+1} \sum_{m=-l}^l K_{n_1, n_2, l, m} K_{n_3, n_4, l, m}, \quad (\text{A4})$$

and

$$\mathcal{I}_{n_1, \dots, n_4}^l = C \int dr' r'^2 R_{n_1}^*(r') R_{n_2}(r') \int dr r^2 R_{n_3}^*(r) R_{n_4}(r) \frac{r_{<}^l}{r_{>}^{l+1}}, \quad (\text{A5})$$

with  $C = e^2/(4\pi\epsilon_0)$ . The values for  $\mathcal{K}_{n_1, \dots, n_4}^l$ , Eq. (A4), can be obtained from the properties and values of the Gaunt coefficients. The radial part, Eq. (A5), can be evaluated by integrating over a sphere of radius  $s$  that has the same volume as a local tetrahedron in the wurtzite crystal [74]:

$$\mathcal{I}_{n_1, \dots, n_4}^l = C \left( \int_0^s dr (r)^{l-1} R_{n_3}^*(r) R_{n_4}(r) \int_0^r dr' (r')^{2+l} R_{n_1}^*(r') R_{n_2}(r') + \int_0^s dr (r)^{2+l} R_{n_3}^*(r) R_{n_4}(r) \int_r^s dr' (r')^{l-1} R_{n_1}^*(r') R_{n_2}(r') \right).$$

We note that based on the Slater rules [71] and the fact that we are considering wave functions at the same lattice site, the radial part will be identical for the four wave functions involved in the above integral [50].

This derivation for evaluating the on-site Coulomb energies allows us now to proceed as follows. Given that the underlying TB framework is an  $sp^3$ -TB model and that when using Slater orbitals the radial function of the localized orbitals is the same, we restrict the spherical expansion to  $l = 0$  ( $s$ -like) contributions. Furthermore, we assume that the wave functions are constant over the sphere around the considered lattice site. In doing so, we find that

$$W_0 = \frac{e^2}{4\pi\epsilon_0} \frac{9}{s} \frac{2}{15}.$$

Evaluating  $W_0$  for InN, we find that  $W_0^{\text{InN}} \approx 16.5$  eV, while for GaN, given the smaller lattice constant compared to InN, we obtain  $W_0^{\text{GaN}} \approx 18$  eV. While further refinements can be made in the evaluation of the on-site energies, these numbers are in good agreement with other calculations of unscreened on-site Coulomb matrix elements [74].

The above numbers for the on-site energy are determined for pure InN and GaN. In an (In,Ga)N/GaN QW, due to alloy fluctuations and strain effects, the volume of the local tetrahedron will vary. To test the impact of the on-site energy on the Auger rate, we have performed calculations using  $W_0^{\text{InN}}$  and  $W_0^{\text{GaN}}$  at low ( $T = 10$  K) and high temperatures ( $T = 300$  K). These test calculations revealed that the  $e$ - $e$ - $h$  Auger coefficient increases by less than 3% at temperatures of 10

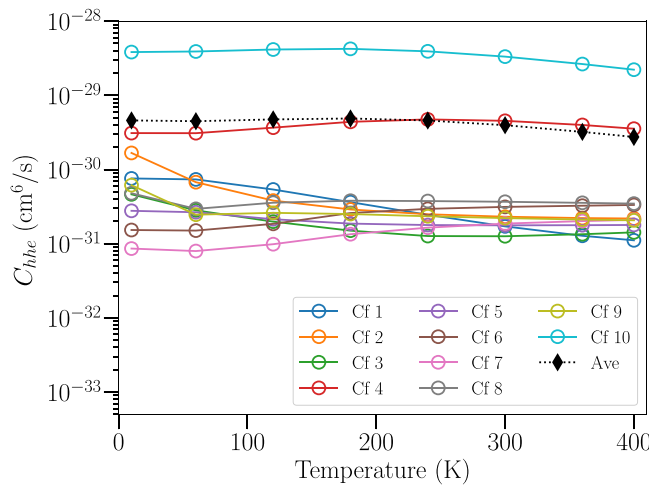


FIG. 6. Auger coefficient,  $C_{hhe}$ , as a function of temperature,  $T$ , for each of the ten different alloy configurations (Cfs) for the 15% In quantum well system. The black diamonds denote the coefficient when averaging over the ten different alloy configurations.

and 300 K when using  $W_0^{\text{GaN}}$  instead of  $W_0^{\text{InN}}$ ; the  $h$ - $h$ - $e$  Auger coefficient increases by less than 13% at the same temperatures again when using  $W_0^{\text{GaN}}$  instead of  $W_0^{\text{InN}}$ . This analysis shows that precise knowledge of the on-site energy is of secondary importance and that the Auger rates are primarily affected by the long-range character of the Coulomb interaction. For all calculations in the main part of the paper we have used  $W_0^{\text{InN}}$ , given that hole wave functions are strongly localized near In-N-In chains [75]. Furthermore, the value  $W_0^{\text{InN}}$  is expected to represent a lower bound on the on-site energies and thus also for the Auger rates. Larger  $W_0$  values will, in general, result in a larger Auger rate compared to values obtained in the main text.

## APPENDIX B: IMPACT OF ALLOY MICROSTRUCTURE ON THE 15% INDIUM QWs

In this Appendix we discuss in more detail the impact of the alloy microstructure on the results for the 15% In QWs studied here. We focus our attention on the hole-hole-electron contribution,  $C_{hhe}$ , as this dominates the total coefficient,  $C_{\text{tot}}$ . Figure 6 depicts the Auger coefficient  $C_{hhe}$  as a function of temperature  $T$ , for each of the ten different random alloy configurations. From this figure it becomes clear that config-

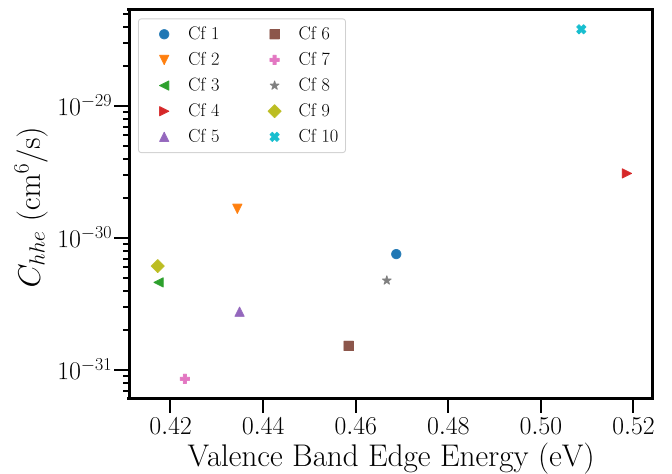


FIG. 7. Auger coefficient,  $C_{hhe}$ , as a function of the valence “band” edge energy (hole ground-state energy) for the ten different alloy configurations (Cfs) of the 15% In quantum well system.

urations (Cfs) 4 and 10 exhibit much larger coefficients than the remaining eight. Also, these two “outliers” do not show a strong temperature dependence and thus do not approach the remaining eight configurations. This results in the situation that the spread in the Auger coefficients remains large at higher temperatures and explains why, in the 15% In case, the spread in the coefficients does not decrease with increasing temperature, as seen in the 10% and 25% In QW systems.

To gain further insight into how the Auger coefficient value,  $C_{hhe}$ , is related to the electronic structure, Fig. 7 shows the  $C_{hhe}$  coefficients for the different alloy configurations with respect to their valence “band” edge (lowest hole ground state) energy at 10 K. As one can see from this plot, the two configurations (Cfs 4 and 10) with the highest Auger coefficient values have the highest valence “band” edge (lowest hole ground state) energy. Such a high valence band energy value is indicative of strong carrier (hole) localization effects [59]. We also find (not shown) that the next valence state (first excited hole state), for both Cfs 4 and 10, has an energy larger than the valence “band” edge energy of the remaining eight configurations. This indicates that not only the hole ground state or valence “band” edge energy but also excited states exhibit strong localization effects. So, even at elevated temperatures, contributions from strongly localized states to the Auger coefficients can arise. The fact that these strongly localized states lead to large Auger coefficients may also support the recently discussed large trap-assisted Auger coefficients [64].

- [1] S. Nakamura, M. Senoh, and T. Mukai, P-GaN/N-InGaN/N-GaN double-heterostructure blue-light-emitting-diode, *Jpn. J. Appl. Phys.* **32**, L8 (1993).
- [2] F. A. Ponce and D. P. Bour, Nitride-based semiconductors for blue and green light-emitting devices, *Nature (London)* **386**, 351 (1997).
- [3] J. Iveland, L. Martinelli, J. Peretti, J. S. Speck, and C. Weisbuch, Direct Measurement of Auger Electrons Emitted from a Semiconductor Light-Emitting Diode under

Electrical Injection: Identification of the Dominant Mechanism for Efficiency Droop, *Phys. Rev. Lett.* **110**, 177406 (2013).

- [4] Y. Fang, L. Wang, Q. Sun, T. Lu, Z. Deng, Z. Ma, Y. Jiang, H. Jia, W. Wang, J. Zhou, and H. Chen, Investigation of temperature-dependent photoluminescence in multi-quantum wells, *Sci. Rep.* **5**, 12718 (2015).
- [5] G. Lin, E. F. Schubert, J. Cho, J. H. Park, and J. K. Kim, Onset of the efficiency droop in GaInN quantum well light-emitting

- diodes under photoluminescence and electroluminescence excitation, *ACS Photonics* **2**, 1013 (2015).
- [6] Y. Park, J. Lim, N. S. Makarov, and V. I. Klimov, Effect of interfacial alloying versus “volume scaling” on Auger recombination in compositionally graded semiconductor quantum dots, *Nano Lett.* **17**, 5607 (2017).
- [7] E. M. T. Fadaly, A. Dijkstra, J. R. Suckert, D. Ziss, M. A. J. van Tilburg, C. Mao, Y. Ren, V. T. van Lange, K. Korzun, S. Kölling, M. A. Verheijen, D. Busse, C. Rödl, J. Furthmüller, F. Bechstedt, J. Stangl, J. J. Finley, S. Botti, J. E. M. Haverkort, and E. P. A. M. Bakkers, Direct-bandgap emission from hexagonal Ge and SiGe alloys, *Nature (London)* **580**, 205 (2020).
- [8] D. A. Wheeler and J. Z. Zhang, Exciton dynamics in semiconductor nanocrystals, *Adv. Mater.* **25**, 2878 (2013).
- [9] E. Kioupakis, P. Rinke, K. T. Delaney, and C. G. Van de Walle, Indirect Auger recombination as a cause of efficiency droop in nitride light-emitting diodes, *Appl. Phys. Lett.* **98**, 161107 (2011).
- [10] K. T. Delaney, P. Rinke, and C. G. Van de Walle, Auger recombination rates in nitrides from first principles, *Appl. Phys. Lett.* **94**, 191109 (2009).
- [11] F. Bertazzi, M. Goano, and E. Bellotti, A numerical study of Auger recombination in bulk InGa<sub>N</sub>, *Appl. Phys. Lett.* **97**, 231118 (2010).
- [12] M. Auf der Maur, A. Pecchia, G. Penazzi, W. Rodrigues, and A. Di Carlo, Efficiency Drop in Green InGa<sub>N</sub>/Ga<sub>N</sub> Light Emitting Diodes: The Role of Random Alloy Fluctuations, *Phys. Rev. Lett.* **116**, 027401 (2016).
- [13] P. Blood, Gain and recombination in quantum dot lasers, *IEEE J. Sel. Top. Quantum Electron.* **15**, 808 (2009).
- [14] J. Piprek, Efficiency droop in nitride-based light-emitting diodes, *Phys. Status Solidi A* **207**, 2217 (2010).
- [15] C. J. Humphreys, Solid-state lighting, *MRS Bull.* **33**, 459 (2008).
- [16] F. Bertazzi, X. Zhou, M. Goano, G. Ghione, and E. Bellotti, Auger recombination in InGa<sub>N</sub>/Ga<sub>N</sub> quantum wells: A full-Brillouin-zone study, *Appl. Phys. Lett.* **103**, 081106 (2013).
- [17] M. Meneghini, C. De Santi, A. Tibaldi, M. Vallone, F. Bertazzi, G. Meneghesso, E. Zanoni, and M. Goano, Thermal droop in III-nitride based light-emitting diodes: Physical origin and perspectives, *J. Appl. Phys.* **127**, 211102 (2020).
- [18] M. Binder, A. Nirschl, R. Zeisel, T. Hager, H. J. Lugauer, M. Sabathil, J. Wagner, D. Bougeard, and B. Galler, Identification of *nnp* and *npp* Auger recombination as significant contributor to the efficiency droop in (GaIn)<sub>N</sub> quantum wells by visualization of hot carriers in photoluminescence, *Appl. Phys. Lett.* **103**, 071108 (2013).
- [19] A. Nirschl, M. Binder, M. Schmid, I. Pietzonka, H. J. Lugauer, R. Zeisel, M. Sabathil, D. Bougeard, and B. Galler, Towards quantification of the crucial impact of Auger recombination for the efficiency droop in (AlInGa)<sub>N</sub> quantum well structures, *Opt. Express* **24**, 2971 (2016).
- [20] A. David, N. G. Young, C. Lund, and M. D. Craven, Review—the physics of recombinations in III-nitride emitters, *ECS J. Solid State Sci. Technol.* **9**, 016021 (2020).
- [21] J. Piprek, Efficiency models for Ga<sub>N</sub>-based light-emitting diodes: Status and challenges, *Materials* **13**, 5174 (2020).
- [22] B. Galler, P. Dreschel, R. Monnard, P. Rode, P. Stauss, S. Froehlich, W. Bergbauer, M. Binder, M. Sabathil, B. Hahn, and J. Wagner, Influence of indium content and temperature on Auger-like recombination in InGa<sub>N</sub> quantum wells grown on (111) silicon substrates, *Appl. Phys. Lett.* **101**, 131111 (2012).
- [23] P. Tian, J. J. D. McKendry, J. HERNSDORF, S. Watson, R. Ferreira, I. M. Watson, E. Gu, A. E. Kelly, and M. D. Dawson, Temperature-dependent efficiency droop of blue InGa<sub>N</sub> micro-light emitting diodes, *Appl. Phys. Lett.* **105**, 171107 (2014).
- [24] F. Nippert, S. Y. Karpov, G. Callsen, B. Galler, T. Kure, C. Nenstiel, M. R. Wagner, M. Strassburg, H.-J. Lugauer, and A. Hoffmann, Temperature-dependent recombination coefficients in InGa<sub>N</sub> light-emitting diodes: Hole localization, Auger processes, and the green gap, *Appl. Phys. Lett.* **109**, 161103 (2016).
- [25] A. David, N. G. Young, C. Lund, and M. D. Craven, Thermal droop in high-quality InGa<sub>N</sub> LEDs, *Appl. Phys. Lett.* **115**, 223502 (2019).
- [26] E. Kioupakis, D. Steiauf, P. Rinke, K. T. Delaney, and C. G. Van de Walle, First principles calculations of indirect Auger recombination in nitride semiconductors, *Phys. Rev. B* **92**, 035207 (2015).
- [27] T. M. Smeeton, M. J. Kappers, J. S. Barnard, M. E. Vickers, and C. J. Humphreys, Electron-beam-induced strain within InGa<sub>N</sub> quantum wells: False indium “cluster” detection in the transmission electron microscope, *Appl. Phys. Lett.* **83**, 5419 (2003).
- [28] J. M. McMahon, D. S. P. Tanner, E. Kioupakis, and S. Schulz, Atomistic analysis of radiative recombination rate, Stokes shift, and density of states in *c*-plane InGa<sub>N</sub>/Ga<sub>N</sub> quantum wells, *Appl. Phys. Lett.* **116**, 181104 (2020).
- [29] D. S. P. Tanner, P. Dawson, M. J. Kappers, R. A. Oliver, and S. Schulz, Polar (In,Ga)<sub>N</sub>/Ga<sub>N</sub> Quantum Wells: Revisiting the Impact of Carrier Localization on the Green Gap Problem, *Phys. Rev. Appl.* **13**, 044068 (2020).
- [30] G. W. ‘t Hooft and C. van Oopdorp, Temperature dependence of interface recombination and radiative recombination in (Al,Ga)As heterostructures, *Appl. Phys. Lett.* **42**, 813 (1983).
- [31] T. Matsusue and H. Sakaki, Radiative recombination coefficient of free carriers in GaAs-AlGaAs quantum wells and its dependence on temperature, *Appl. Phys. Lett.* **50**, 1429 (1987).
- [32] C. M. Jones, C.-H. Teng, Q. Yan, P.-C. Ku, and E. Kioupakis, Impact of carrier localization on recombination in InGa<sub>N</sub> quantum wells and the efficiency of nitride light-emitting diodes: Insights from theory and numerical simulations, *Appl. Phys. Lett.* **111**, 113501 (2017).
- [33] A. Di Vito, A. Pecchia, A. Di Carlo, and M. Auf der Maur, Impact of Compositional Nonuniformity in (In,Ga)<sub>N</sub>-Based Light-Emitting Diodes, *Phys. Rev. Applied* **12**, 014055 (2019).
- [34] D. Chaudhuri, M. O’Donovan, T. Streckenbach, O. Marquardt, P. Farrell, S. K. Patra, T. Koprucki, and S. Schulz, Multiscale simulations of the electronic structure of III-nitride quantum wells with varied indium content: Connecting atomistic and continuum-based models, *J. Appl. Phys.* **129**, 073104 (2021).
- [35] J. Hader, J. V. Moloney, and S. W. Koch, Temperature-dependence of the internal efficiency droop in Ga<sub>N</sub>-based diodes, *Appl. Phys. Lett.* **99**, 181127 (2011).
- [36] S. Y. Karpov, Carrier localization in InGa<sub>N</sub> by composition fluctuations: Implication to the “green gap”, *Photon. Res.* **5**, A7 (2017).
- [37] A. David, N. G. Young, and M. D. Craven, Compensation between radiative and Auger recombinations in III-nitrides: The scaling law of separated-wavefunction recombinations, *Appl. Phys. Lett.* **115**, 193502 (2019).

- [38] I. E. Titkov, S. Y. Karpov, A. Yadav, V. L. Zerova, M. Zulonas, B. Galler, M. Strassburg, I. Pietzonka, H.-J. Lugauer, and E. U. Rafailov, Temperature dependent internal quantum efficiency of blue high-brightness light-emitting diodes, *IEEE J. Quantum Electron.* **50**, 911 (2014).
- [39] S. F. Chichibu, A. Uedono, T. Onuma, B. A. Haskell, A. Chakraborty, T. Koyama, P. T. Fini, S. Keller, S. P. DenBaars, J. S. Speck, U. K. Mishra, S. Nakamura, S. Yamaguchi, S. Kamiyama, H. Amano, I. Akasaki, J. Han, and T. Sota, Origin of defect-insensitive emission probability in In-containing (Al,In,Ga)N alloy semiconductors, *Nat. Mater.* **5**, 810 (2006).
- [40] P. Dawson, S. Schulz, R. A. Oliver, M. J. Kappers, and C. J. Humphreys, The nature of carrier localisation in polar and non-polar InGaN/GaN quantum wells, *J. Appl. Phys.* **119**, 181505 (2016).
- [41] M. A. Caro, S. Schulz, and E. P. O'Reilly, Theory of local electric polarization and its relation to internal strain: Impact on the polarization potential and electronic properties of group-III nitrides, *Phys. Rev. B* **88**, 214103 (2013).
- [42] S. Schulz, M. A. Caro, C. Coughlan, and E. P. O'Reilly, Atomistic analysis of the impact of alloy and well width fluctuations on the electronic and optical properties of InGaN/GaN quantum wells, *Phys. Rev. B* **91**, 035439 (2015).
- [43] D. M. Graham, A. Soltani-Vala, P. Dawson, M. J. Godfrey, T. M. Smeeton, J. S. Barnard, M. J. Kappers, C. J. Humphreys, and E. J. Thrush, Optical and microstructural studies of InGaN/GaN single-quantum-well structures, *J. Appl. Phys.* **97**, 103508 (2005).
- [44] L. Rigutti, B. Bonaf, J. Speck, F. Tang, and R. A. Oliver, Atom probe tomography of nitride semiconductors, *Scr. Mater.* **148**, 75 (2018).
- [45] D. Watson-Parris, M. J. Godfrey, P. Dawson, R. A. Oliver, M. J. Galtrey, M. J. Kappers, and C. J. Humphreys, Carrier localization mechanisms in  $\text{In}_x\text{Ga}_{1-x}\text{N}/\text{GaN}$ , *Phys. Rev. B* **83**, 115321 (2011).
- [46] D. T. S. Watson-Parris, Carrier localization in InGaN/GaN quantum wells, Ph.D. thesis, University of Manchester, 2011.
- [47] H. Haug and S. W. Koch, *Quantum Theory of the Optical and Electronic Properties of Semiconductors*, 3rd ed. (World Scientific, Singapore, 2001).
- [48] G. G. Zegrya and A. D. Andreev, Mechanism of suppression of Auger recombination processes in type-II heterostructures, *Appl. Phys. Lett.* **67**, 2681 (1995).
- [49] A. D. Andreev and G. G. Zegrya, Theoretical study of thresholdless Auger recombination in compressively strained InAlAsSb/GaSb quantum wells, *Appl. Phys. Lett.* **70**, 601 (1997).
- [50] S. Schulz, S. Schumacher, and G. Czycholl, Tight-binding model for semiconductor quantum dots with a wurtzite crystal structure: From one-particle properties to Coulomb correlations and optical spectra, *Phys. Rev. B* **73**, 245327 (2006).
- [51] W. Sheng, S. J. Cheng, and P. Hawrylak, Multiband theory of multi-exciton complexes in self-assembled quantum dots, *Phys. Rev. B* **71**, 035316 (2005).
- [52] K. Schuh, S. Barthel, O. Marquardt, T. Hickel, J. Neugebauer, G. Czycholl, and F. Jahnke, Strong dipole coupling in nonpolar nitride quantum dots due to Coulomb effects, *Appl. Phys. Lett.* **100**, 092103 (2012).
- [53] S. Barthel, K. Schuh, O. Marquardt, T. Hickel, J. Neugebauer, F. Jahnke, and G. Czycholl, Interplay between Coulomb interaction and quantum-confined Stark-effect in polar and nonpolar wurtzite InN/GaN quantum dots, *Eur. Phys. J. B* **86**, 449 (2013).
- [54] N. Baer, S. Schulz, S. Schumacher, P. Gartner, G. Czycholl, and F. Jahnke, Optical properties of self-organized wurtzite InN/GaN quantum dots: A combined atomistic tight-binding and full configuration interaction calculation, *Appl. Phys. Lett.* **87**, 231114 (2005).
- [55] M. Zieliński, Multi-scale simulations of semiconductor nanostructures, *Acta Phys. Pol. A* **122**, 312 (2012).
- [56] E. Kioupakis, Q. Yan, and C. G. V. de Walle, Interplay of polarization fields and Auger recombination in the efficiency droop of nitride light-emitting diodes, *Appl. Phys. Lett.* **101**, 231107 (2012).
- [57] M. Hajdel, M. Chlipała, M. Siekacz, H. Turski, P. Wolny, K. Nowakowski-Szkudlarek, A. Feduniewicz-Żmuda, C. Skierbiszewski, and G. Muziol, Dependence of InGaN quantum well thickness on the nature of optical transitions in LEDs, *Materials* **15**, 237 (2022).
- [58] G. Muziol, M. Hajdel, M. Siekacz, H. Turski, K. Pieniak, A. Bercha, W. Trzeciakowski, R. Kudrawiec, T. Suski, and C. Skierbiszewski, III-nitride optoelectronic devices containing wide quantum wells—unexpectedly efficient light sources, *Jpn. J. Appl. Phys.* **61**, SA0801 (2022).
- [59] D. S. P. Tanner, M. A. Caro, E. P. O'Reilly, and S. Schulz, Random alloy fluctuations and structural inhomogeneities in  $c$ -plane  $\text{In}_x\text{Ga}_{1-x}\text{N}$  quantum wells: Theory of ground and excited electron and hole states, *RSC Adv.* **6**, 64513 (2016).
- [60] A. David, N. G. Young, and M. D. Craven, Many-Body Effects in Strongly Disordered III-Nitride Quantum Wells: Interplay Between Carrier Localization and Coulomb Interaction, *Phys. Rev. Applied* **12**, 044059 (2019).
- [61] G. M. Christian, S. Schulz, M. J. Kappers, C. J. Humphreys, R. A. Oliver, and P. Dawson, Recombination from polar InGaN/GaN quantum well structures at high excitation carrier densities, *Phys. Rev. B* **98**, 155301 (2018).
- [62] G. M. Christian, S. Schulz, S. Hammersley, M. J. Kappers, M. Frentrup, C. J. Humphreys, R. A. Oliver, and P. Dawson, Optical properties of  $c$ -plane InGaN/GaN single quantum wells as a function of total electric field strength, *Jpn. J. Appl. Phys.* **58**, SCCB09 (2019).
- [63] S. Schulz, D. P. Tanner, E. P. O'Reilly, M. A. Caro, T. L. Martin, P. A. J. Bagot, M. P. Moody, F. Tang, J. T. Griffiths, F. Oehler, M. J. Kappers, R. A. Oliver, C. J. Humphreys, D. Sutherland, M. J. Davies, and P. Dawson, Structural, electronic, and optical properties of  $m$ -plane InGaN/GaN quantum wells: Insights from experiment and atomistic theory, *Phys. Rev. B* **92**, 235419 (2015).
- [64] A. David, N. G. Young, C. A. Hurni, and M. D. Craven, Quantum Efficiency of III-Nitride Emitters: Evidence for Defect-Assisted Nonradiative Recombination and its Effect on the Green Gap, *Phys. Rev. Applied* **11**, 031001(R) (2019).
- [65] D. J. Myers, A. C. Espenlaub, K. Gelzinyte, E. C. Young, L. Martinelli, J. Peretti, C. Weisbuch, and J. S. Speck, Evidence for trap-assisted Auger recombination in MBE grown InGaN quantum wells by electron emission spectroscopy, *Appl. Phys. Lett.* **116**, 091102 (2020).
- [66] D. Schiavon, M. Binder, M. Peter, B. Galler, P. Drechsel, and F. Scholz, Wavelength-dependent determination of the

- recombination rate coefficients in single-quantum-well GaInN/GaN light emitting diodes, *Phys. Status Solidi B* **250**, 283 (2013).
- [67] P. G. Eliseev, The red  $\sigma^2/kT$  spectral shift in partially disordered semiconductors, *J. Appl. Phys.* **93**, 5404 (2003).
- [68] A. Alkauskas, C. E. Dreyer, J. L. Lyons, and C. G. Van de Walle, Role of excited states in Shockley-Read-Hall recombination in wide-band-gap semiconductors, *Phys. Rev. B* **93**, 201304(R) (2016).
- [69] S. Lee, L. Jönsson, J. W. Wilkins, G. W. Bryant, and G. Klimeck, Electron-hole correlations in semiconductor quantum dots with tight-binding wave functions, *Phys. Rev. B* **63**, 195318 (2001).
- [70] S. Lee, J. Kim, L. Jönsson, J. W. Wilkins, G. W. Bryant, and G. Klimeck, Many-body levels of optically excited and multiply charged InAs nanocrystals modeled by semiempirical tight binding, *Phys. Rev. B* **66**, 235307 (2002).
- [71] J. C. Slater, Atomic shielding constants, *Phys. Rev.* **36**, 57 (1930).
- [72] J. D. Jackson, *Classical Electrodynamics* (Wiley, New York, 1975).
- [73] Y.-L. Xu, Fast evaluation of the Gaunt coefficients, *Math. Comput.* **65**, 1601 (1996).
- [74] I. Schnell, G. Czycholl, and R. C. Albers, Hubbard- $U$  calculations for Cu from first-principle Wannier functions, *Phys. Rev. B* **65**, 075103 (2002).
- [75] P. R. C. Kent and A. Zunger, Carrier localization and the origin of luminescence in cubic InGaN alloys, *Appl. Phys. Lett.* **79**, 1977 (2001).